

Rotating diamonds with embedded spins in a magnetic field

Marc VAN DEN BOSSCHE¹ and supervised by Gabriel HÉTET²

¹Département de Physique, École Normale Supérieure, 75005 Paris.

²Laboratoire Pierre Aigrain, École Normale Supérieure, PSL Research University, CNRS, Université Pierre et Marie Curie, Sorbonne Universités, Université Paris Diderot, Sorbonne Paris-Cité, 24 rue Lhomond, 75231 Paris Cedex 05, France.

From June, 25th to July, 20th of 2018

Abstract

Here we first study the general properties of NV-centres in a diamond and the properties of the PAUL trap used to levitate microdiamonds. We then focus on the techniques that are used to probe the spin of NV-centres and the mechanical properties of the microdiamonds. After that we show that the laser-induced rotation of a microdiamond requires a minimal confinement of the diamond, and propose a model for the PAUL-trap influenced rotation of microdiamonds taking the gyroscopic stabilisation into account. Finally we try to fit the experimentally measured influence of a magnetic field on a rotating spin with a perturbation theory.

Dans ce rapport, nous étudions d'abord les propriétés générales des centres NV dans le diamant et du piège de PAUL utilisé pour la lévitation de microdiamants. Nous nous attacherons ensuite aux techniques utilisées couramment pour sonder les spins des centres NV et les propriétés mécaniques des microdiamants. Nous montrons ensuite que la rotation par laser d'un micro-diamant ne peut avoir lieu qu'à partir d'un certain niveau de confinement et nous proposons un modèle de rotation pour la rotation d'un micro-diamant influencée par le piège de PAUL en tenant compte de la stabilisation gyroscopique. Enfin, nous essayons d'expliquer, à l'aide d'une méthode perturbative, l'influence d'un champ magnétique sur un spin en rotation.

Contents

Introduction	2
1 The general experimental set-up	3
1.1 General overview of the set-up	3
1.2 The PAUL trap	3
1.3 NV-diamonds	5
1.3.1 General description	5
1.3.2 Energy states	5
2 Experimental techniques	7
2.1 Rabi oscillation measurement	7
2.2 Ramsey decay measurement	8
2.3 Echo measurement	9
2.4 ESR	10
2.5 Measuring the rotation speed	11
2.5.1 Retroreflection	11
2.5.2 Photoluminescence photon count	11
2.5.3 ESR spectroscopy	11
2.5.4 Frequency analysis	11
3 General experimentally observed properties of the set-up: microdiamond rotation	13
3.1 Micromovement	13
3.1.1 Positional destabilisation	13
3.1.2 Angular destabilisation	13
3.2 Rotation of a particle due to radiation pressure	13
3.2.1 Influence of the laser power	13
3.2.2 Dependency on the trap frequency	14
3.2.3 Dependency on the trap AC voltage amplitude	15
3.2.4 Dependency on the trap offset	15
3.2.5 The influence of an external electric static field	16
3.2.6 Air pressure dependency	16
3.3 Conclusion: A model for microdiamond rotation	18
4 Rotating NV-centres in a magnetic field	20
4.1 Rotation of a spin-1 system in a magnetic field	20
4.2 Measuring the magnetic field with spins	22
4.2.1 Calibrating the system	22
4.2.2 Using the spins	23
4.2.3 Seeing the rotation using ESR spectroscopy	23
Appendix	26
Breakdown voltage of air and plasmas	26
Bibliography	27
Acknowledgements	28

Introduction

This is the report of my four-week internship in the team *optique cohérente et non-linéaire* supervised by Gabriel HÉTET. This internship began with me visiting the lab almost every Friday afternoon since March 2018. Then there were four non-stop weeks from June, 25th until July, 20th. On the Friday afternoons I started to get to know the team and the experiment. Then the four weeks have been dedicated to the core of the experimental work.

Context

The study of NV-centre physics belongs at the same time to solid state physics and cold-atom physics. Solid state physics because we have to take into account the electron energy band and gaps of the diamond lattice, its defects and the phonons degrees of freedom. They are also very close to cold-atom physics because one also has to consider the energy levels of a small number of such defects in the lattice at a time. Furthermore the states of these defects also have a very long decoherence time (up to milliseconds) at room temperature. This long coherence time enables working with the spin of a NV-centre using π , $\frac{\pi}{2}$... pulses as in cold-atom physics.

Long run applications

One of the possible future uses of NV-centres is Qbits thanks to their long coherence time and the way in which they are easily handled. However it is also very interesting to work on achieving a controlled spin-phonon coupling in order to explore fundamental physics. It is for example possible to cool the diamond by removing the phonons of the lattice using their coupling with NV-centre which can be optically manipulated. It is also possible (and we will see it) to measure an external magnetic field using the spin of a NV-centre and research is being done to explore metrological applications, such as studying the geometric phase of a quantum system [9] because a rotating microdiamond is a good system to study geometric phase as a spin rotates slowly on a close contour and thus accumulates a phase in a static magnetic field [10]. It is also crucial to understand well the gyroscopic stabilisation of levitating rotating microdiamond in order to understand the rotation mechanism.

Subject

In order to be able to explore all the above mentioned applications, one has to master the mechanism behind the rotation of a levitating rotation microdiamond. Hence, the subject of this work has been the study of the mechanical rotating of microdiamonds with NV-centres levitating in a PAUL trap, the limitations of the rotation and its dependency on the trap parameters. This allows studying a rotating spin-1 system undergoing a mechanically controlled rotation in a fixed static magnetic field. This opposes the approach, where spins are fixed in a rotating magnetic field.

Chapter 1

The general experimental set-up

1.1 General overview of the set-up

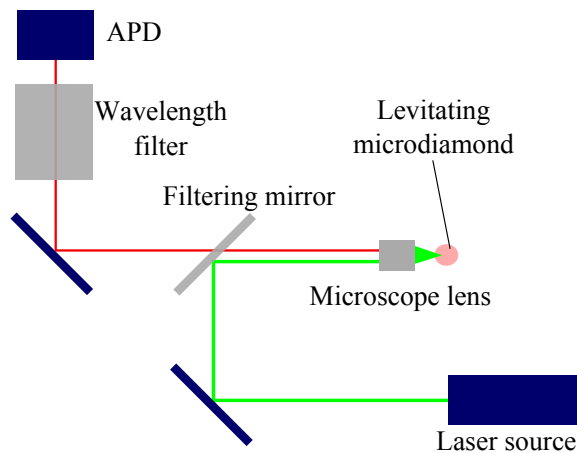


Figure 1.1: The general overview of the set-up. The laser is used to light the levitating diamond trapped in a PAUL trap. The reflected light or the red photoluminescence (see subsection 1.3.2.) can then be collected with an APD. Some of the green light is not filtered by the filtering mirror hence the necessity of using a specific wavelength filter.

At the beginning of the internship, there was one set-up where the trap was in a vacuum chamber. As we were between two and four working on the same set-up, I eventually made an other one next to the first on the optical table. It has enable us working on more than one experiment and measurement at a time and thus working faster.

1.2 The PAUL trap

To levitate a micro-diamond, we trap it in a PAUL trap. Such a trap enables us trapping small charged particles such as micro-diamonds. The induced potential is the following

$$V = \frac{U}{\Omega} \cos(\Omega t) (a_x x^2 + a_y y^2 + a_z z^2),$$

where U is the amplitude of the applied AC voltage and Ω its frequency. a_x , a_y and a_z are constants constrained by the LAPLACE law $\Delta V = 0$ in the vacuum, thus $a_x + a_y + a_z = 0$. That is why the potential is saddle-shaped. A DC voltage can also be applied to compensate for gravity.

The induced potential is saddle shaped and the particle is trapped. This indeed traps the particle but as external forces (such as gravity, collisions with gaz particles...) constantly pulls the trapped particle downwards or sideways, it is possible (and often the case) that the trapped particle oscillates. This oscillation is called "micro-movement" and its frequency is that of the trap

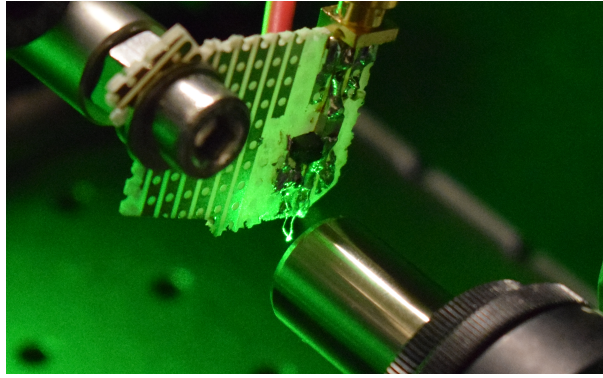


Figure 1.2: One of the PAUL trap we used in front of a microscope lens.

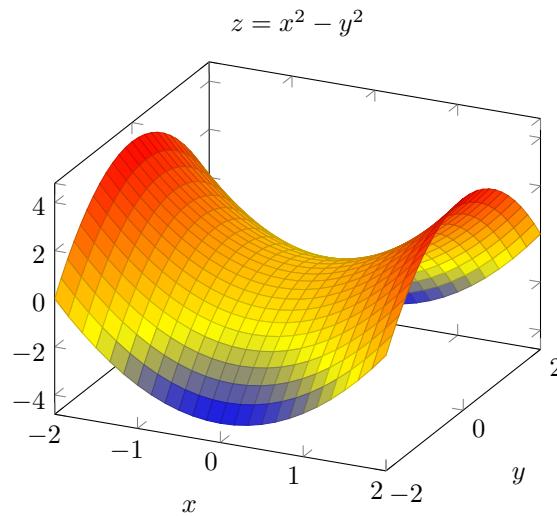


Figure 1.3: Saddle shaped potential of the PAUL trap in two dimensions when time is frozen. The units are arbitrary. The real potential is of course in three dimensions, but it is easier to understand with only two.

Something to be wary of using a PAUL trap with low pressure, is that a plasma can be created if the voltage U is too high (and exceeds the breakdown voltage of air). This can damage the trap significantly and is to be avoided by decreasing the voltage as air pressure goes down (see appendix for the voltage and pressure conditions that should be avoided). The breakdown happens between the trap and an other part of the set-up. It might be the microscope lens or some metallic piece depending on the set-up.

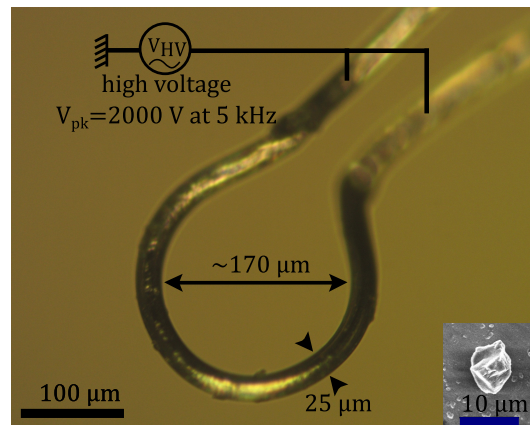


Figure 1.4: A PAUL trap from closer. In order to build one, we twist the $25 \mu\text{m}$ wire around a thicker one (to make the loop) and then with a clamp, we make the “bottle-neck” opening.

1.3 NV-diamonds

1.3.1 General description

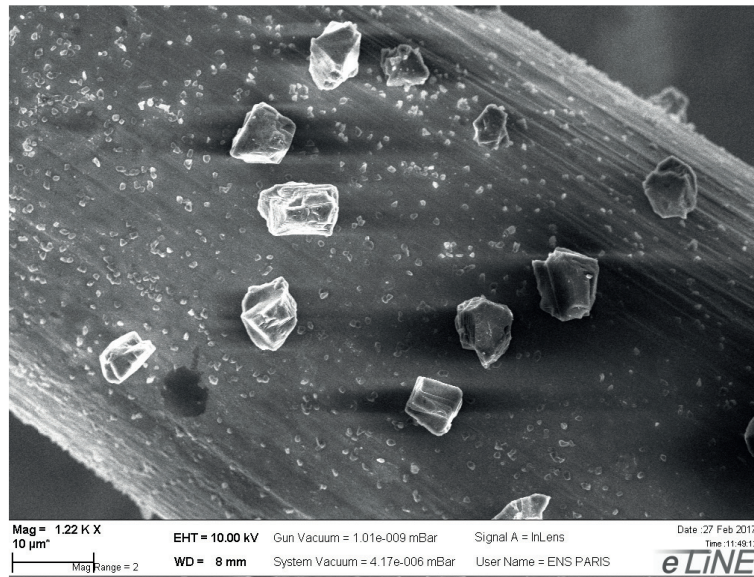


Figure 1.5: Picture of microdiamonds taken with Electronic Sweeping Microscope (ESM)¹. The size of the microdiamonds we used were between 2 μm and 12 μm depending on the chosen sample.

Here we will use mostly NV-diamonds. NV-diamonds are diamonds (with their regular tetraedric carbon lattice) where some of the carbon atoms have been replaced by Nitrogen atoms (N). As nitrogen can only have three covalent bonds, there is a vacant site besides it (V).

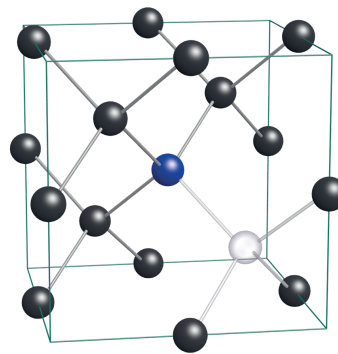


Figure 1.6: An NV centre in a diamond lattice. The nitrogen atom is depicted in blue and the vacancy is in grey. The black atoms are the carbon atoms of the diamond lattice.

1.3.2 Energy states

Nitrogen has five valence electrons but only three of them can be part of a covalent bond. The two other electrons are part of a lone pair. The system we study is a negatively ionised NV centre : an NV^- centre (but we will refer to them as “NV-centres”, we will no longer be mentioning the negative charge). This centre is composed of the two electrons of the lone pair, the three electrons from the surrounding carbon atoms and the one from the ionisation.

This system can be described by a spin one system, which states are $|m = -1\rangle$, $|m = 0\rangle$ and $|m = +1\rangle$. Unless otherwise indicated, those states will be referred to as $|-1\rangle$, $|0\rangle$ and $|+1\rangle$.

We will consider that the pair of carbon atoms that are being replaced with an NV centre are randomly chosen. Hence, as the diamond lattice is tetrahedral, there are four possible orientations for an NV centre.

¹Some of the pictures used in this report, such as this one, were kindly provided by the team and are used with their consent.

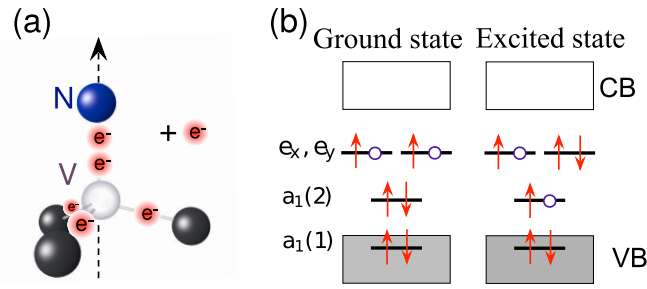


Figure 1.7: NV centre energy levels and electrons, from [8].

When lit up with a green light, the NV-centre spontaneously emits a very dim red light. This light can not be seen with the naked eye, but can be measured using an APD (Avalanche Photo Diode : single photon counter).

The ground level on the previous figure corresponds to the 3A_2 triplet and the excited level is the 3E triplet depicted on fig. 1.8. Those two levels are strongly coupled through electrical dipolar transition (which conserves the spin).

The ground and excited triplets are also coupled by non-radiative transitions through the two metastable singlets 1A_1 and 1E (even though they are spin-1 states). The lifetimes of these states are indicated on fig. 1.8. The fact that 3A_2 and 3E are also coupled in this way reduces photoluminescence.

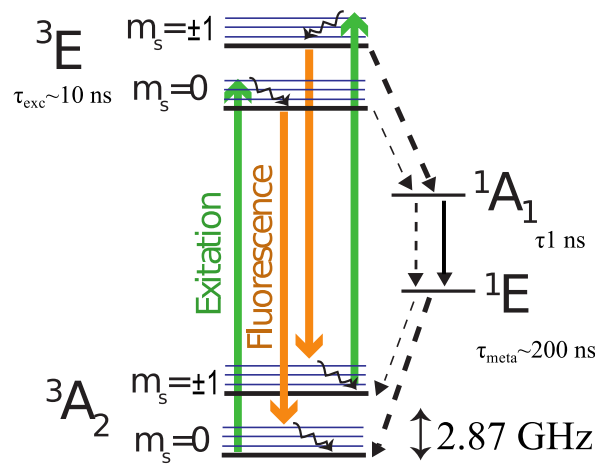


Figure 1.8: NV centre energy structure and photoluminescence. The thicker the arrow, the higher the transition rate is. Going through the metastable states **does not preserve the spin** of the electron.

There is a cunning way to measure the spin of the system using the metastable energy levels. This is possible because the transition rate of the metastable states strongly depends on the spin of the electron and because the desexcitation through the metastable state does not preserve the spin of the electron. The two dependencies are the following:

- The transition from $^3E \rightarrow ^1A$ is favoured when the electron is in one of the $|m = \pm 1\rangle$ states.
- The transition from $^1E \rightarrow ^3A$ has a favoured output : the $|m = 0\rangle$ state.

As indicated on fig. 1.8 by the thickness of the arrows representing the transitions, the electrons in the state $^3E|m = \pm 1\rangle$ are more likely to desexcitate through the metastable states than the electrons in the state $^3E|m = 0\rangle$. Then, the spin of the electron is not conserved when desexcitating through the metastable states and the output state of this desexcitation is more likely to be $^3A|m = 0\rangle$ than $^3A|\pm 1\rangle$.

This means that if we do the $^3A \rightarrow ^3E$ transition for a long time, we achieve a spin polarisation of the system (80% will be in the state $|m = 0\rangle$) using a microwave tone tuned close to 2.87 GHz. This can then be used to manipulate the spin of the system at will as well as reading the spin state.

Chapter 2

Experimental techniques

2.1 Rabi oscillation measurement

The RABI oscillations measurement is useful to tune the π and $\frac{\pi}{2}$ pulses that are often used. They consist in measuring the population in each state (for a two-level system) using the photoluminescence after sending a resonating wave (such that $E_2 - E_1 = \hbar\omega$) during a time interval of length τ .

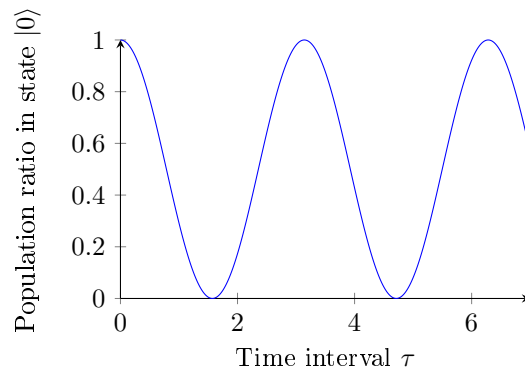


Figure 2.1: A perfect Rabi oscillation plot would look like that if there were no decoherence (arbitrary units of time). Yet that is not what we observe. The τ_π time that would enable to induce a π pulse is easy to read as it is the time at which the population has been totally shifted from state $|0\rangle$ to $|1\rangle$: it is the time at which the population in state $|0\rangle$ equals zero for the first time.

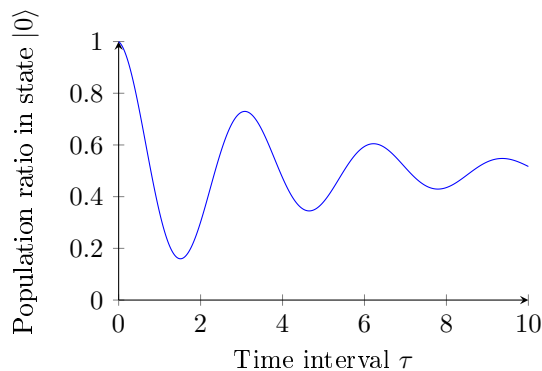


Figure 2.2: A Rabi oscillation plot with decoherence (arbitrary units of time) looks like this one. If the oscillations are fast enough, it is still possible to read the τ_π time : it is the time at which the population in state $|0\rangle$ is at a minimum for the first time. The time describing the exponential decay is called T_1 .

The time that would induce a $\frac{\pi}{2}$ pulse is easy to deduce from the τ_π time since it is half of that time.

$$\tau_{\frac{\pi}{2}} = \frac{\tau_\pi}{2}$$

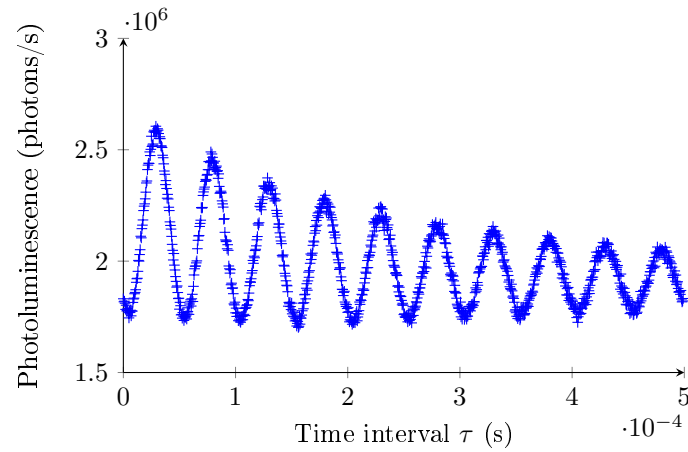


Figure 2.3: Here is an experimentally measured Rabi oscillation plot. We use the photoluminescence which informs us about the population distribution.

2.2 Ramsey decay measurement

RAMSEY decay measurements are useful to study the environment of the system we observe. This measurement consist in two $\frac{\pi}{2}$ pulses with a delay τ in between. If we use the BLOCH sphere representation, after the first pulse, the system is be in the equatorial plane of the sphere. Here we will wait for a time τ and the environment modifies the position of the vector representing the system in the sphere. After the second pulse, (if we make the measurement many times) it is possible to measure the influence of the environment on the system as is should always modify the vector in a similar way.

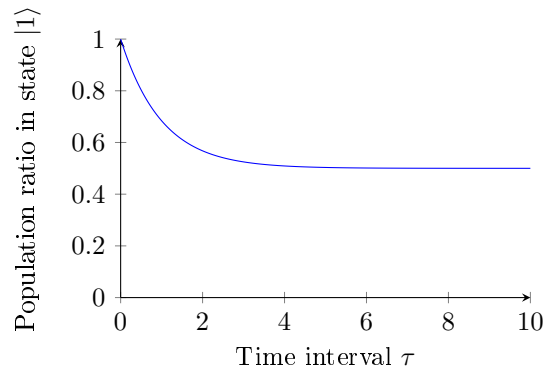


Figure 2.4: This how a Ramsey measurement looks like. If we wait a long time the system becomes a statistical superposition of both states. The time describing the exponential decay is called T_2 and describes the influence on the environment of the system.

If the microwave used for the $\frac{\pi}{2}$ pulses is slightly detuned, there will be oscillations on the measured photoluminescence rate.

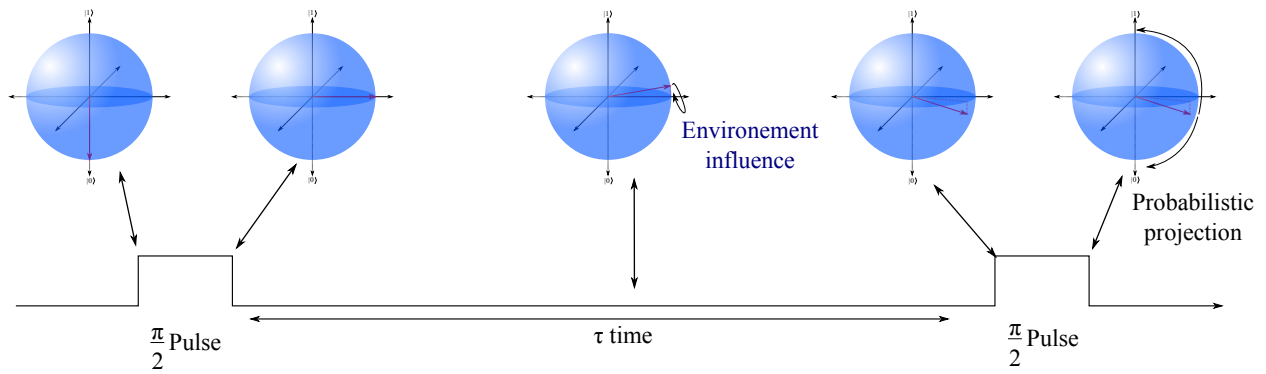


Figure 2.5: The BLOCH sphere representation of the Ramsey measurement.

2.3 Echo measurement

An echo measurement is very similar to a RAMSEY measurement but it is useful to see the long-time environment influence, which the RAMSEY measurement can not see. The idea is simple: if one does a π pulse around another axis of the bloch sphere in the middle of a Ramsey sequence, the “short-time” noise will be canceled. The sequence is the following : First a $\frac{\pi}{2}$ pulse, then wait for a time (which we will again call τ), then a π pulse, then wait for τ , and finally the last $\frac{\pi}{2}$ pulse. We then measure the proportion of the population in each state using photoluminescence.

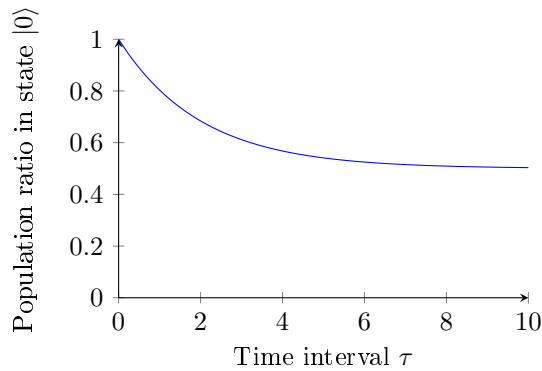


Figure 2.6: This how an echo measurement looks like. If we wait for a long time the system becomes a statistical superposition of both states here as well. The exponential decay time is called T_2^* and describes the influence of the environment of the system in the long run.

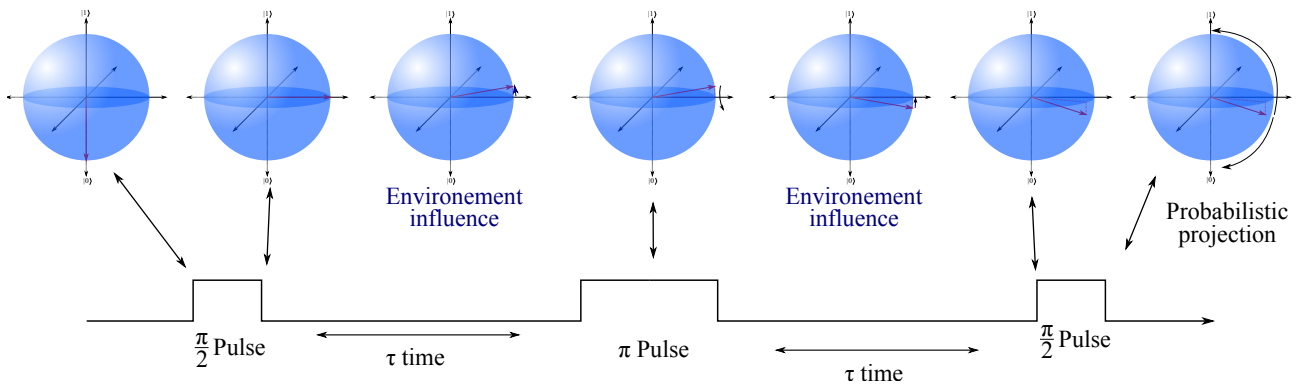


Figure 2.7: The BLOCH sphere representation of the echo measurement.

The Echo measurement can be used to measure the influence of the other spins of the diamond. For instance some isotopes of nitrogen (^{14}N) and of carbon (^{13}C) are present and will have an influence on the system *via* their nuclear spins. The coherence time of such spins is huge in comparison to the one of the NV centre. They can reach coherence times as long as days or even weeks !

2.4 ESR

The ESR (Electronic Spin Resonance) spectroscopy is a way to scan the states of the NV-centres. It is a photoluminescence scan as the frequency of a microwave varies. The wire that emits the microwave is the one of the trap.

Example on the NV-centre:

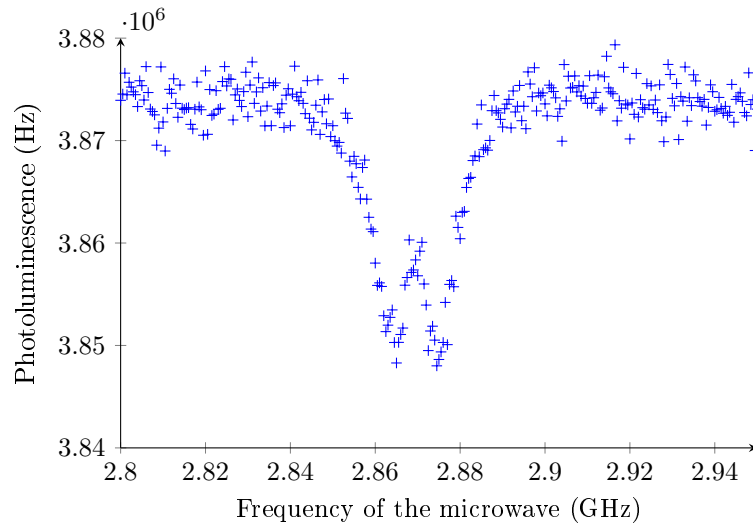


Figure 2.8: ESR without magnetic field.

We can see on the previous ESR spectrum that there are two peaks instead of one. The reason is that there is strain inside the diamond bulk and this slightly lifts the degenerescence of the $| - 1 \rangle$ and $| + 1 \rangle$ states.

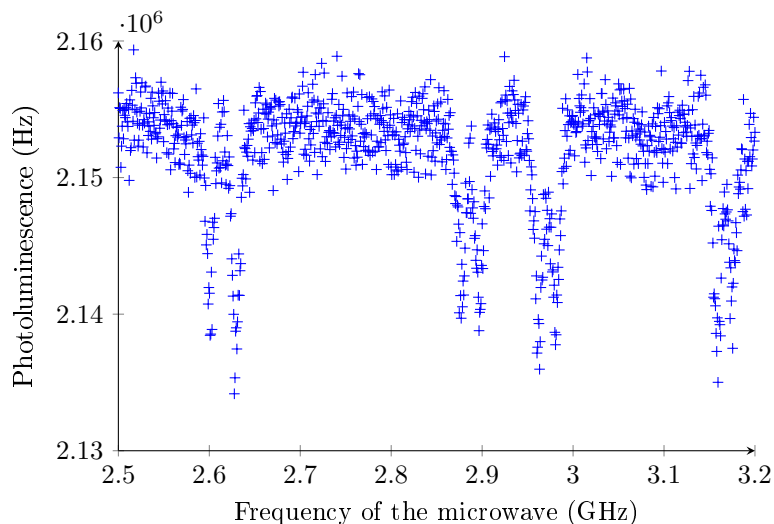


Figure 2.9: ESR with magnetic field : we can see the Zeemann effect. The eight spots we observe correspond to the $| - 1 \rangle$ and $| + 1 \rangle$ states of each possible orientation of the NV-centres.

The parameters of an ESR spectrum are :

- The frequency width (but the microwave generator can not output a frequency higher than 3.2 GHz).

- The amplitude of the amplification of the microwave (a higher amplification will give a better contrast but the wire of the trap will heat up and move).
- The number of sampling points on the given frequency width (the higher the better but the longer).
- The time spent on each point (a longer time will give out a better averaging, hence less noise).

The previous plots are obtained thanks to multiples measures done on a single microdiamond containing NV-centres. Each point is an average on time (because we choose the time spent on scanning the photoluminescence on each frequency point) and a statistical average (because the scan over the frequency span is done multiple times - generally between 100 and 10.000 times).

2.5 Measuring the rotation speed

We would like to understand the rotation of a levitating diamond induced by the radiation pressure on the faces of the micro-diamond. Hence we need to measure the rotation speed.

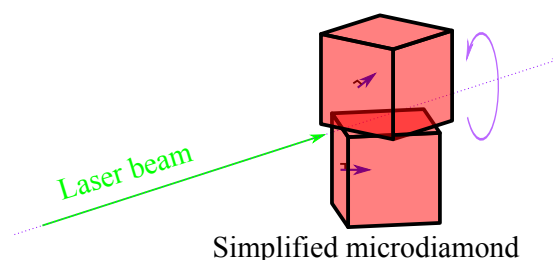


Figure 2.10: When lit with an intense light (for instance laser light) a diamond with a lot irregular faces will act in the same way as a windmill in the wind. The blue inward arrows coming from the cube faces represent the normal component of the radiation pressure force on the facet. The purple arrow represent the rotation of the diamond due to the overall torque induced by the radiation pressure on its many facets.

2.5.1 Retroreflection

The first idea that comes to the mind to measure the rotational speed is to measure the light reflected on the micro-diamond as a function of time. Even if the intensity might be a bit chaotic, it should be periodic as the diamond rotates. To do this, one has to plug the photon count signal from the APD directly to a spectrum analyser and the peak corresponding to the rotation of the levitating particle will be clear.

This method works well and is particularly useful when the diamond has a low photoluminescence rate or when using micro iron spheres. The problem with this method is that we can only have information about rotation. It is not possible to do ESR spectroscopy while using this technique because we can not distinguish the intense reflected light from the dim red photoluminescence.

2.5.2 Photoluminescence photon count

An other way to measure the rotation speed is to measure the photoluminescence of the NV-sites of the micro-diamond, using the already existing set-up. The diamonds rotate and the NV-centres rotate along with them. As they do so the diamond is being lit up with a green laser. Thus the photoluminescence will vary periodically at the same rate as the diamond rotates. Using the photoluminescence can be difficult because the number of NV-centre in a microdiamond can vary a lot and sometimes the photoluminescence is very weak and indistinguishable from noise.

2.5.3 ESR spectroscopy

See subsection 4.2.3.

2.5.4 Frequency analysis

When using the retroreflection or the photoluminescence photon count methods, it is possible to plug the output signal on a spectrum analyser.

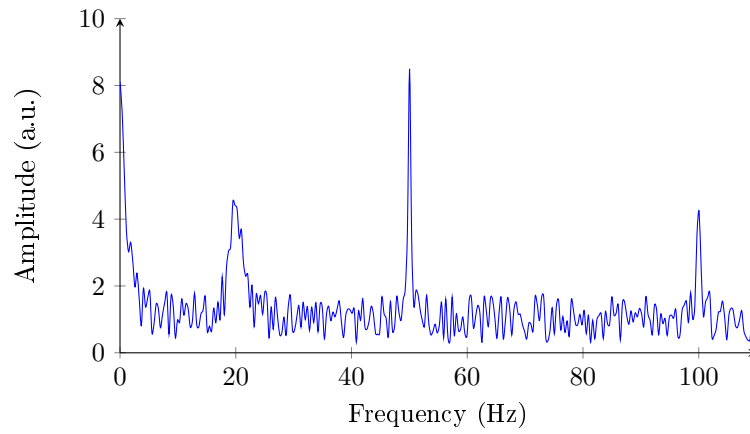


Figure 2.11: This is what a frequency spectrum looks like. It is all the more easy to spot the peak corresponding to the rotation of the diamond, that most of the time the rotation can be seen with the naked eye thanks to the light going through the set-up (and we see the shadow of the diamond). This is also a way of checking the order of magnitude of the rotation frequency. We can also very clearly see the peaks at 50 Hz and 100 Hz corresponding to the French domestic AC power network.

Chapter 3

General experimentally observed properties of the set-up: microdiamond rotation

3.1 Micromovement

The PAUL trap induces a trapping potential which rotates with time. This rotation can induce a movement of the particle around the center of the trap. We call this instability *micromovement*. This instability is of the center of mass, but also of the angle of the trapped particle.

3.1.1 Positional destabilisation

The first thing that is noticeable is that the frequency of the micromovement of the center of mass due to the trap is the one of the trap (and the first harmonics as well). This is something to be wary of, because the amplitude of the micromovement is often bigger than the amplitudes of other phenomena and it might be mistaken for something else.

3.1.2 Angular destabilisation

The angular micromovement is trickier to measure because its amplitude is much smaller than the amplitude of the positional micromovement. It is also not easy to distinguish the angular movement of a moving particle.

3.2 Rotation of a particle due to radiation pressure

Sometimes, when a particle is trapped inside the PAUL trap, we observe that it begins to rotate when we change some of the trap's parameters. We guess that this rotation is mostly due to the radiation pressure of the laser on the particle but we would like to have a precise model of this rotation.

Applying the angular momentum conservation to the rotation particle, we get that:

$$J\ddot{\theta} = -\Gamma\dot{\theta} + C.$$

Where J is the angular mass of the microdiamond, θ its angle with a given axis, Γ the damping rate caused by various elements (such as the air viscosity) and C is the torque induced by the radiation pressure of the laser used to light the diamond.

If the diamond reaches a stable rotational state with $\ddot{\theta} = 0$, we hence have the rotation speed ω such that:

$$\omega = \frac{C}{\Gamma}.$$

3.2.1 Influence of the laser power

The radiation pressure is proportional to the number of incoming photons on the microdiamond. As such, the torque should also be proportional to it and hence to the laser power. This is confirmed by the measurement plotted on fig. 3.1.

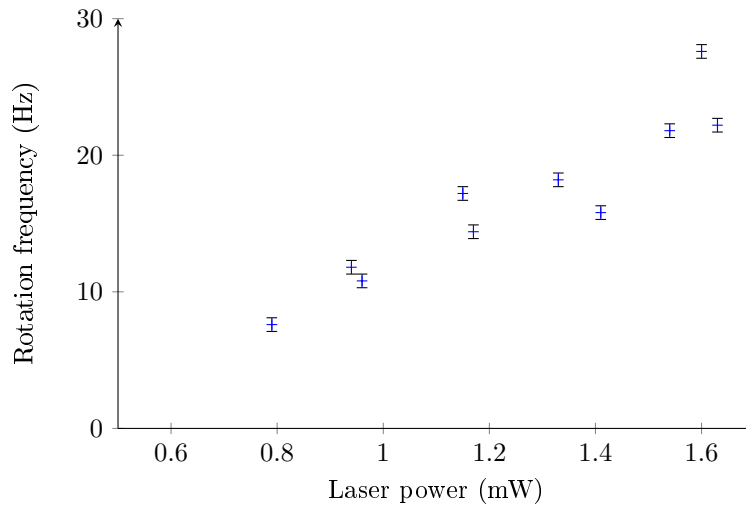


Figure 3.1: Rotation frequency as a function of the laser power. This seems to be proportional as expected. The error comes from the width of the peak on the frequency metre.

It is important to note that the position of the levitating microparticle relative to the focal point of the laser seems to play a role as can be seen looking at fig. 3.2.

This might be caused by a the movement of the center of mass of the particle rather than some angular rotation.

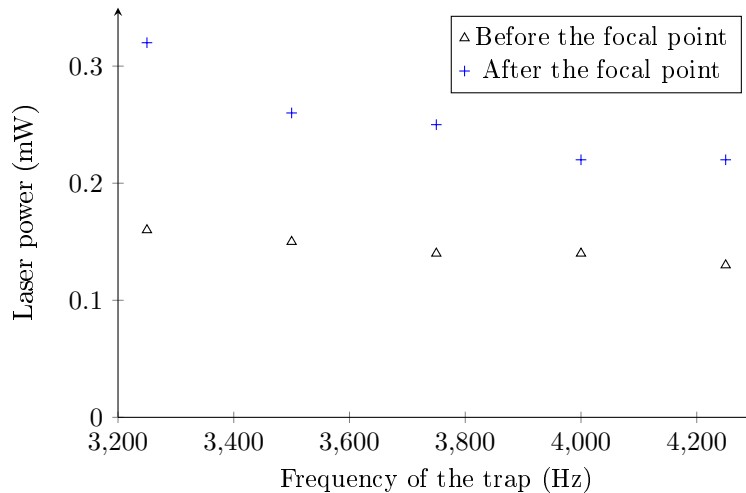


Figure 3.2: Minimal laser power that induces a rotation of the trapped levitating microdiamond at a given trap frequency. The power seems to be slightly higher at low frequency and stable afterwards. The errors are ± 0.01 mW.

One idea was that the microdiamond is pushed outwards the trap when after the focal point and that the microdiamond is pushed inwards the trap when before the focal point. If this hypothesis is true, that would mean that as the microdiamond is less confined by the trap when after the focal point, more laser power is needed for it to rotate. Still the effect of the position relatively to the focal point is not very important here.

3.2.2 Dependency on the trap frequency

The hypothesis is that when the trap is tighter (Ω is small) the particle is confined in a better way in the center of the trap, the angular and positional micromovement are thus reduced and the main dependency of the rotation are radiation pressure and air damping, *i.e.* at low Ω , the rotation does not depend on the trap frequency.

As shown on fig. 3.3, with a lower confinement, the particle is more instable and thus the rotation speed decreases and when the destabilisation is too high in comparison to the radiation pressure, the particle stops rotating.

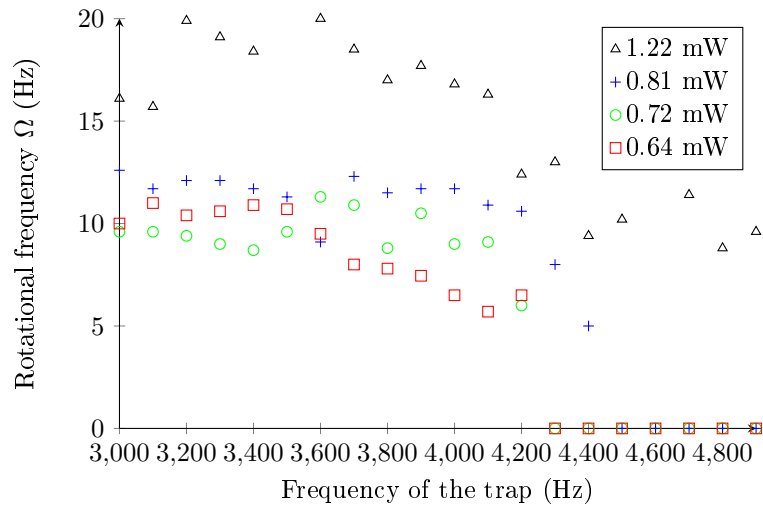


Figure 3.3: Influence of the trap frequency on the rotation frequency. We see that as the trap frequency gets bigger, the rotation speed of the particle first stays about constant and then rapidly decreases until it stops rotating. The errors are ± 0.5 Hz.

3.2.3 Dependency on the trap AC voltage amplitude

An other adjustable parameter of the PAUL trap is the amplitude of the AC voltage U we choose to apply. We know that the potential induced by the trap is directly proportional to U , but we do not know anything about the relation of this amplitude with the rotational speed of a trapped particle.

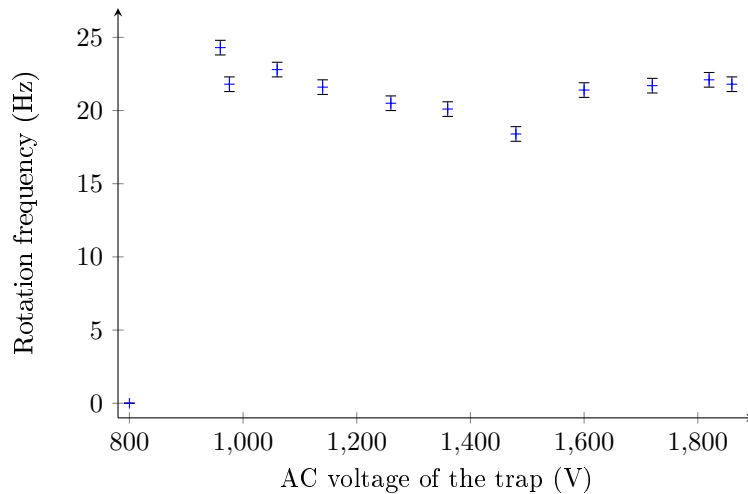


Figure 3.4: Measured rotation frequency as a function of the AC voltage applied to the PAUL trap. We can see that with 800 V, the levitating diamond does not rotate. After it begins rotating, the rotation frequency seems to be pretty stable.

As we saw with the measurement (see fig. 3.4), the particle rotation seems to be independent of the AC amplitude. Yet the particle started to rotate at a given voltage, which could mean that in order to achieve rotation, the particle has to be trapped in an efficient way.

3.2.4 Dependency on the trap offset

A voltage with an offset value can also be applied to the trap. What is experimentally observed when we choose to apply an offset is that the particle moves vertically in the trap. The explanation for that is that the levitating particle is charged (or else it could not be trapped) and the trap is not perfectly symmetrical in the vertical direction (there is “less” trap at the top because there is a so called “bottle neck”). When the offset is set to a negative value the particle (almost always) goes up (because the diamonds charge negatively). A well tuned offset can compensate perfectly the gravity action on the levitating particle.

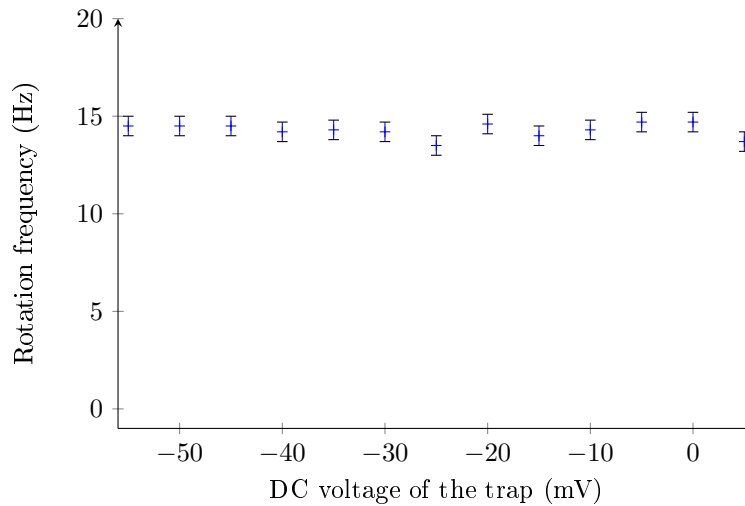


Figure 3.5: Here is plotted a measurement of the rotation speed of a levitating diamond as a function of the Offset value of the voltage applied to the trap. It seem to be even more stable than with the AC voltage.

Although the offset value of the voltage applied to the trap has an influence on the equilibrium position of the particle in the trap, the rotation speed seem not to be influenced by it (see fig. 3.5).

3.2.5 The influence of an external electric static field

We saw that the micromovement induced a vibration of the particle. One might want to cancel it. An idea for that is to apply an external static electric field on the particle. This could stabilise the particle. Here we tried to apply a DC voltage on the lens rim (which was made of non-magnetic metal).

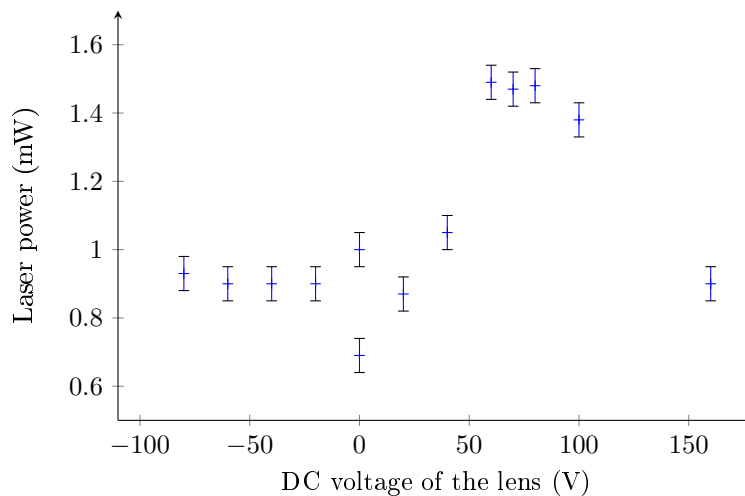


Figure 3.6: Here is plotted the minimal laser power that induces a rotation for a given DC voltage applied to the lens rim. Some voltage values are missing on the plot because it was sometimes hard to see whether the particle was rotating as it was very unstable and its shadow very dim.

3.2.6 Air pressure dependency

We studied the damping rate dependency in air pressure. The link between rotation speed and the damping is the following :

$$\omega = \frac{C}{\Gamma},$$

where Γ is the damping rate and C is the torque due to radiation pressure.

Here we try different theoretical models of fluid-induced damping in order to fit the experimentally measured damping plotted on fig. 3.7.

Damping rate and air pressure

According to [2], the damping rate should depend on the air pressure as follows:

$$\Gamma = \frac{6\pi\eta r}{m} \frac{0.619}{0.619 + \text{Kn}} \left(1 + \frac{0.31\text{Kn}}{0.785 + 1.25\text{Kn} + \text{Kn}^2} \right),$$

where Γ is the damping due to the air, η is the viscosity of air, r the size of the particle, m its mass and the KNUDSEN number Kn is defined as $\text{Kn} = \frac{\ell}{r}$, where ℓ is the mean free path in the fluid.

The KNUDSEN number can be rewritten in such a way that the pressure dependency becomes visible:

$$\text{Kn} = \frac{k_B T}{P \sigma r},$$

where k_B is the BOLTZMANN constant, T the temperature, P the pressure, σ the effective cross-sectional area for collision and r the size of the particle. For our system, we have $\text{Kn} \approx 1$ (*i.e.* the KNUDSEN number is neither very small in comparison to 1, nor very large), thus we can not make any approximation concerning the KNUDSEN number.

This model does unfortunately not fit the experimental measurements.

Viscosity pressure dependency

As the simple pressure dependency seems not to explain the phenomenon we observe, we look into a pressure dependency of viscosity. G.M. Pančkov proposes in [3] a pressure dependency of fluid viscosity, which is the following:

$$\eta = 3\sqrt{6R} \sqrt[3]{\frac{w^2}{N_0} \frac{\rho^{\frac{4}{3}}}{M^{\frac{5}{6}}}} \sqrt{T} e^{\varepsilon/RT} (1 - e^{\varepsilon/RT})^2.$$

Where R is the ideal gas constant, w is the volume of a mole of the fluid, N_0 the LOSCHMIDT constant, ρ is the fluid density, M is the molecular weight and ε is the binding energy of the fluid molecules. The link with pressure appears through the density : $\rho = \frac{PM}{RT}$. Hence, we have :

$$\eta = cst \times P^{\frac{4}{3}}.$$

This model does not fit either (when coupled to the previous one).

An other model for the pressure dependency of the viscosity has been proposed by [5] and used by [4] for microparticle rotation in vacuum:

$$\eta = \frac{\eta_0}{1 + 9.638 \text{Kn}^{1.159}},$$

where η_0 is a constant (viscosity at $T = 0\text{K}$).

Using a model derived from this one, we managed to fit the experimental data. The slightly modified model is:

$$\eta = \frac{\eta_0}{1 + a \left(\frac{b}{P}\right)^c},$$

where the fitting parameters are η_0 , a , b and c .

The experimentally measured dependency on air pressure is the following

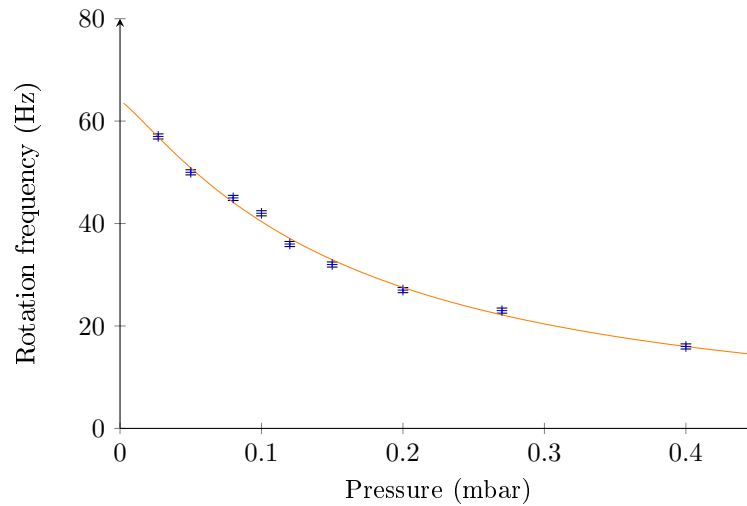


Figure 3.7: Experimental measure dependency on air pressure of the rotation frequency and the fit with $(a, b, c, \eta_0) = (1.1469 \times 10^9, 7.5154 \times 10^6, -1.1799, 63.97507)$ which does not make much sense... We expected order of magnitude close to the one proposes in [5] and $\eta_0 \approx 10^{5-6}$.

It is possible that at low pressure the rotation of the diamond is induced by the micromovement as well as the laser radiation pressure. This would explain that no simple theoretical prediction fits the observed pressure dependency.

3.3 Conclusion: A model for microdiamond rotation

Now that the dependency of the rotation mode on a lot of parameters of the trap has been probed, it is possible to propose a model for it.

The first thing that we can deduce from de observations is that the rotation is induced by the radiation pressure of the laser as we guessed. The microdiamond rotates because it is not perfectly spherical. It is a piece of crystal with angular facets as explained by fig. 2.10.

What we can deduce from our observations is that the particle can not rotate if its confinement is too loose. As for the dependency on the trap parameters, rotation seems to be relatively stable.

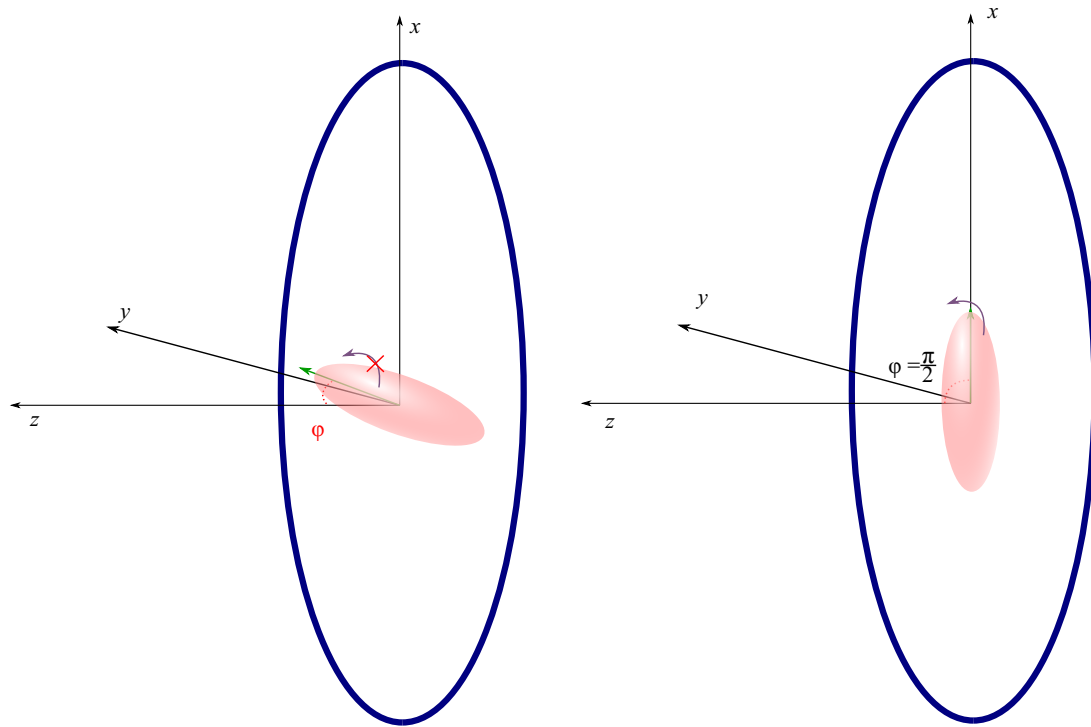


Figure 3.8: An hypothetical way of seeing the rotation. If the φ angle is too small because the confinement is not tight enough, the particle will not rotate because the angle is not stabilised and the angle will wobble (left). If the confinement is tight enough, the particle will be able to rotate around the z axis without wobbling (right).

This gyroscopic stabilisation can also be understood with an usual rotating system that would tend to have its biggest dimension (in fact the dimension with the biggest angular mass) perpendicular to the rotation axis. It is the same physical phenomenon as with a rotating spinning top. When it spins around an axis (for example the z axis like on the figure above) the rotations around the other axes are stabilised (around x and y). Thanks to this efficient stabilisation, both geometric phase measurement and spin-mechanical coupling are made easier.

It is possible that, at low pressure, the φ angle is modified and the diamond still rotates due to a combination of micromovement and radiation pressure effects.

We could try to find a combination of the trap parameters that would account for the trapping quality for which a critical value would trigger the stability of the rotation. This number should take into account the different angular masses of the diamond and the trap parameters (and even perhaps the ambient air pressure).

Chapter 4

Rotating NV-centres in a magnetic field

In this chapter we will study the properties of a rotating spin-1 system in a static magnetic field. We consider that the state transitions are adiabatic.

4.1 Rotation of a spin-1 system in a magnetic field

Let us consider a spin-1 system of two electrons. This system is not rotation invariant since there are two electrons. As we saw earlier, this is a three level system, two of which are degenerate ($|m = -1\rangle$, $|m = 0\rangle$ and $|m = +1\rangle$). The hamiltonian of this system (without magnetic field), which explains the degenerescence of the $|m = -1\rangle$ and $|m = +1\rangle$ states, is

$$\hat{H} = -JS_z^2.$$

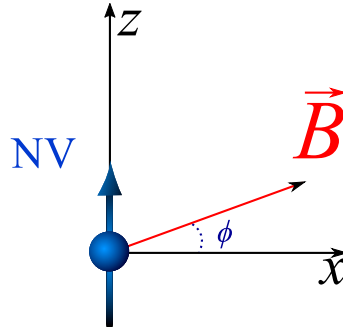


Figure 4.1: The spins are along the z axis and the magnetic field \mathbf{B} is in the xz plane.

We choose to work in the basis in which the spin operator along the z axis is diagonal. With such a point of view, we have:

$$|-1\rangle = \begin{pmatrix} 0 \\ 0 \\ 1 \end{pmatrix} \quad |0\rangle = \begin{pmatrix} 0 \\ 1 \\ 0 \end{pmatrix} \quad |1\rangle = \begin{pmatrix} 1 \\ 0 \\ 0 \end{pmatrix}.$$

For this system, we define three axe x , y and z each associated to the spin-1 system operator $\hat{\mathbf{S}}$ such that :

$$S_x = \begin{pmatrix} 0 & 1 & 0 \\ 1 & 0 & 1 \\ 0 & 1 & 0 \end{pmatrix}, S_y = \begin{pmatrix} 0 & -1 & 0 \\ 1 & 0 & -1 \\ 0 & 1 & 0 \end{pmatrix} \text{ and } S_z = \begin{pmatrix} 1 & 0 & 0 \\ 0 & 0 & 0 \\ 0 & 0 & -1 \end{pmatrix}.$$

z being the axis of the spins as shown on fig. 4.1

We apply a magnetic field \mathbf{B} to the system and we wish to know how the states will evolve. We choose to use cylindrical coordinates where ϕ is the angle between the magnetic field and the x -axis.

Thus, the hamiltonian of the system is the following :

$$\hat{H} = -JS_z^2 + \gamma\hat{\mathbf{S}} \cdot \mathbf{B}.$$

$\gamma\widehat{\mathbf{S}} \cdot \mathbf{B}$ is the spin-field coupling term. We suppose that $|\gamma\mathbf{B}| \ll J$ in order to apply perturbation theory. The final energy states will thus be slight modification of E_0 , for $|0\rangle$, and E_1 , for both states $|\pm 1\rangle$. Let us split our hamiltonian in two and look at the coupling part: $\widehat{H}_c = \gamma\widehat{\mathbf{S}} \cdot \mathbf{B}$.

This problem is rotation invariant around the z axis, let us name ϕ the angle between the plane orthogonal to z and \mathbf{B} . Choosing an x axis in this plane, we hence have :

$$\widehat{H}_c = \gamma B \left(\cos \phi \widehat{S}_x + \sin \phi \widehat{S}_z \right),$$

and in a matricial point of view:

$$\widehat{H}_c = \gamma B \begin{pmatrix} \sin \phi & \frac{\cos \phi}{\sqrt{2}} & 0 \\ \frac{\cos \phi}{\sqrt{2}} & 0 & \frac{\cos \phi}{\sqrt{2}} \\ 0 & \frac{\cos \phi}{\sqrt{2}} & -\sin \phi \end{pmatrix}$$

Let us write ε the new energy levels found using perturbation theory. We will solve the problem using perturbation theory at the first order.

We have, for the first level:

$$\begin{aligned} \varepsilon_0 &= E_0 + \langle 0 | \widehat{H}_c | 0 \rangle \\ &= E_0 \end{aligned}$$

We choose to use the perturbation theory at the second order since the first order does not change ε_0 . We hence have, for the first level:

$$\begin{aligned} \varepsilon_0 &= \sum_{i \in \{-1, 1\}} \frac{|\langle 0 | \widehat{H}_c | i \rangle|^2}{-E_i} \\ &= \frac{(\gamma B)^2}{E_1} \cos^2(\phi) \end{aligned}$$

For the other level, we have to find the ε that enables us solving the following two equations:

$$\begin{cases} (\varepsilon - D) \alpha_1 = \sum_{i \in \{-1, 1\}} \left[\langle 1 | \widehat{H}_c | i \rangle + \frac{\langle 1 | \widehat{H}_c | 0 \rangle \langle 0 | \widehat{H}_c | i \rangle}{E_i} \right] \alpha_i \\ (\varepsilon - D) \alpha_{-1} = \sum_{i \in \{-1, 1\}} \left[\langle -1 | \widehat{H}_c | i \rangle + \frac{\langle -1 | \widehat{H}_c | 0 \rangle \langle 0 | \widehat{H}_c | i \rangle}{E_i} \right] \alpha_i \end{cases}$$

where $D = E_1 - E_0$. By choosing $E_0 = 0$, we have $E_1 = D$. This system is equivalent to:

$$\begin{pmatrix} D - \varepsilon + \gamma B \sin \phi + (\gamma B)^2 \frac{\cos^2 \phi}{2D} & (\gamma B)^2 \frac{\cos^2 \phi}{2D} \\ (\gamma B)^2 \frac{\cos^2 \phi}{2D} & D - \varepsilon - \gamma B \sin \phi + (\gamma B)^2 \frac{\cos^2 \phi}{2D} \end{pmatrix} \begin{pmatrix} \alpha_1 \\ \alpha_{-1} \end{pmatrix} = \begin{pmatrix} 0 \\ 0 \end{pmatrix}.$$

In order to have non-trivial solution, we choose to look at when the determinant of the matrix is 0. Hence we have the equation on ε :

$$\left(D - \varepsilon + \gamma B \sin \phi + (\gamma B)^2 \frac{\cos^2 \phi}{2D} \right) \left(D - \varepsilon - \gamma B \sin \phi + (\gamma B)^2 \frac{\cos^2 \phi}{2D} \right) - (\gamma B)^4 \frac{\cos^4 \phi}{4D^2} = 0,$$

whose solutions are:

$$\varepsilon_{\pm} = D + (\gamma B)^2 \frac{\cos^2 \phi}{2D} \pm \gamma B \sqrt{\frac{(\gamma B)^2 \cos^4 \phi}{4D^2} + \sin^2 \phi}.$$

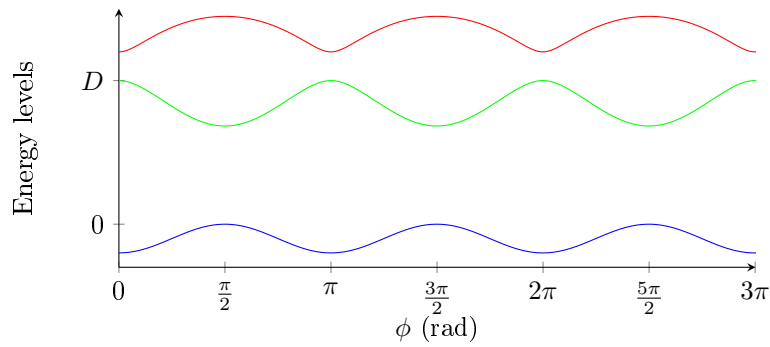


Figure 4.2: The energy levels in arbitrary units as a function of the angle ϕ

It is important to notice that if the energy levels change with the angle ϕ *i.e.* the eigenvalues of the hamiltonian, the eigenstates also change with ϕ . We use the $\{|m = -1\rangle, |m = 0\rangle, |m = +1\rangle\}$ basis to describe them. And we name them in the following way :

$|g\rangle$: the “ground” state which is the state with the lowest energy (its energy is plotted in blue on fig. 4.2).

$|e\rangle$: the “excited” state whose energy is the highest (its energy is plotted in red on fig. 4.2).

$|d\rangle$: the intermediate state (its energy is plotted in green on fig. 4.2).

Each one of these eigenstates can be written in the previously chosen basis, as a linear combination of $|m = -1\rangle$, $|m = 0\rangle$ and $|m = +1\rangle$.

4.2 Measuring the magnetic field with spins

As we saw with the ESR, the system is sensitive to the magnetic field through the ZEEMANN effect. It is thus possible to measure the magnetic field using this effect.

4.2.1 Calibrating the system

First we have to calibrate the system with a known magnetic field. In order to do that, we measure the magnetic field as a function of the distance of a magnet using a HALL effect probe.

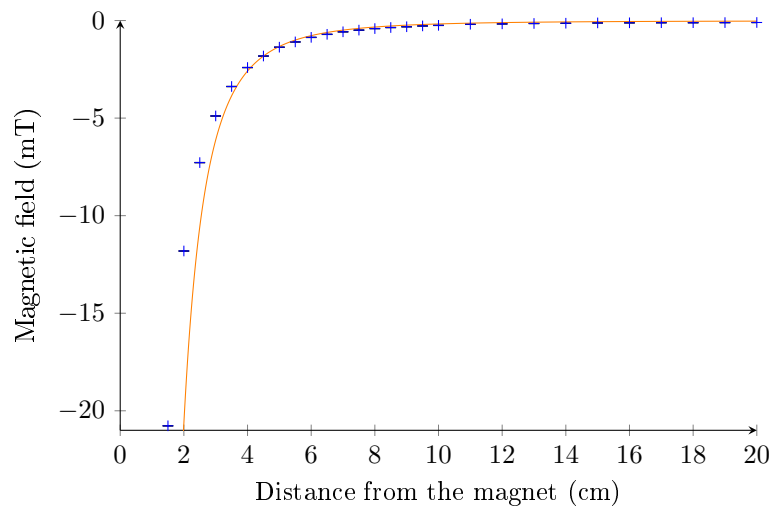


Figure 4.3: Magnetic field as a function of the distance to the magnet. In orange is plotted the expected $B = \frac{a}{r^3} + b$ fit. There is a slight difference near the magnet because it is not a perfect dipole and at this distance, the imperfection is no longer neglectible.

With this plot we will be able to compare the obtained result with the spins and the one with the HALL effect probe which should be more reliable.

4.2.2 Using the spins

We can now measure the ZEEMANN splitting as a function of the distance of the magnets (there are now two magnets like the one which magnetic field we measured with the probe in the previous section).

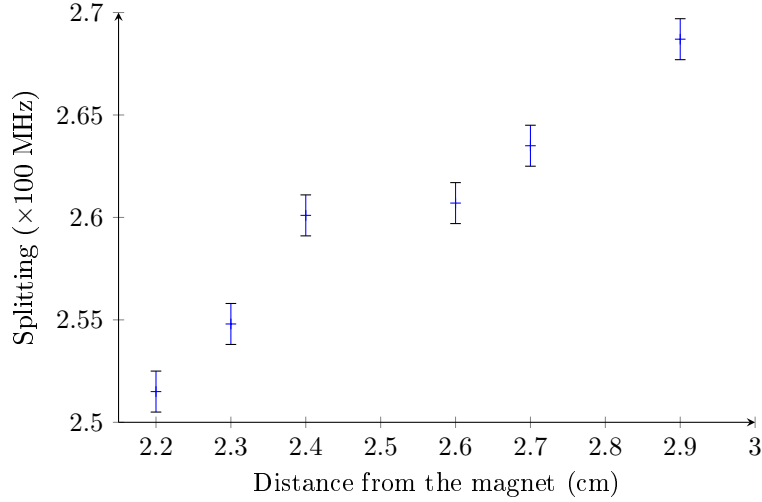


Figure 4.4: This is the ZEEMANN splitting between the centremost peaks on a ESR spectrum as a function of the distance of the magnets to the trap. The splitting should be proportional the magnetic field.

We can find the magnetic field using the previous plot but an easier way would be to use the calculation of the previous section.

We know that:

$$\begin{cases} \varepsilon_- = D + (\gamma B)^2 \frac{\cos^2 \phi}{2D} - \gamma B \sqrt{\frac{(\gamma B)^2 \cos^4 \phi}{4D^2} + \sin^2 \phi} \\ \varepsilon_+ = D + (\gamma B)^2 \frac{\cos^2 \phi}{2D} + \gamma B \sqrt{\frac{(\gamma B)^2 \cos^4 \phi}{4D^2} + \sin^2 \phi} \end{cases}$$

Those values are the ones measured with the peaks on an ESR. But we can further simplify, with Δ and Σ respectfully the values of the difference and sum of ε_- and ε_+ .

$$\begin{cases} \Delta = 2\gamma B \sqrt{\frac{(\gamma B)^2 \cos^4 \phi}{4D^2} + \sin^2 \phi} \\ \Sigma = 2D + (\gamma B)^2 \frac{\cos^2 \phi}{D} \end{cases}$$

Here we simply solve the system for B and ϕ (using Mathematica for example). And we find some disturbing results :

For example using the following ESR :

We find:

$$\begin{cases} B \simeq 28.12 \text{ mT} \\ \phi \simeq 0.1239i \text{ rad} \end{cases}$$

While the imaginary angle is rather odd, the magnetic field is of the right order of magnitude (in comparison to what we measured with the HALL effect probe).

This imaginary value might be due to the fact that we used a perturbation theory to derive the energy level values while the magnetic field might not be small enough for the perturbation theory to hold.

4.2.3 Seeing the rotation using ESR spectroscopy

It is also possible to see the rotation (although it is hard to extract data from it) on ESR spectrum. The peak is spread on the whole spectra according to the arcsine distribution because the axis of the NV-centres in the diamond bulk will rotate with the microdiamond.

It is interesting to note that if a magnetic field is applied in the same axis that the one of the rotation, the magnetic field seen by the NV-centres will not change during the rotation. I did not have the time to do such a measurement.

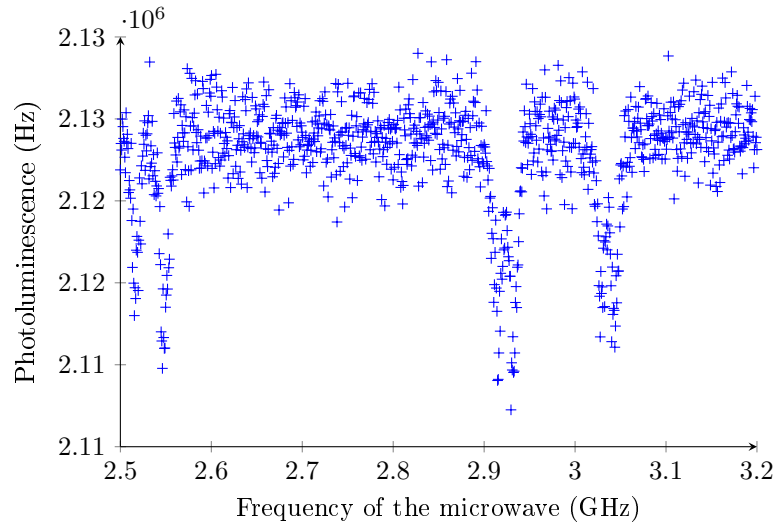


Figure 4.5: ESR with magnetic field. For the central peaks : $\Delta = 100$ MHz and $\Sigma = 596$ MHz.

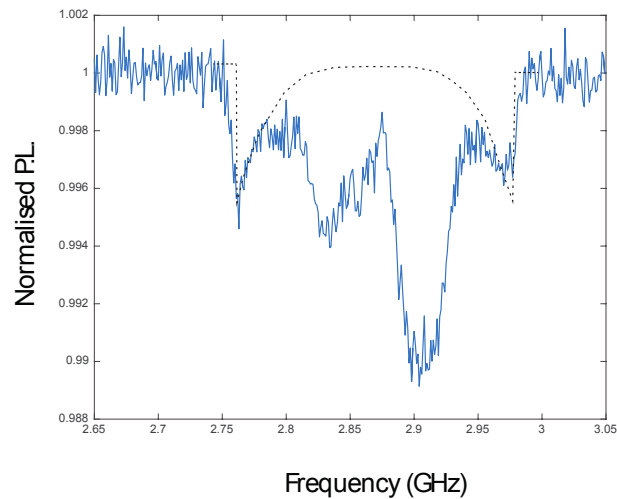


Figure 4.6: ESR with a magnetic field with a rotation microdiamond. We can see that the peak shape changes and on the right we can see the arcsine distribution.

Conclusion

During this internship I worked mainly on studying the rotation properties of microdiamonds and the rotation of the spins in their defects. I first got familiar with the experimental techniques that are being daily used in this team and that are very close to cold-atom physics ones. It was also a good way to feel the decoherence and the ZEEMANN effect from a hands-on point of view. I then focused on characterising the experimentally-observed properties of the set-up that were not well studied yet, such as the rotation of microdiamonds in a PAUL trap and its dependency on every parameter of the trap. This has enabled suggesting a model for the rotation of the microdiamond. This model can be further studied for confirmation. Once the characterisation of the set-up done, I could work with a static magnetic field and study its influence on the NV-centre spin-1 system. The results that I got through measurement did not agree with the one from the calculations but it has been a way to see that a perturbative approach of the spin hamiltonian is not suited here.

Now that the rotation has been understood, we can consider applying the metrology ideas (measuring the geometric phase for instance) to the levitating NV-diamond system.

This experiment has enabled me working in fundamental physics, very close to cold-atoms, while keeping a foot in solid-state physics. The advantage of doing so is that, in comparison to cold-atom physics experiments, the set-up for this experiment was relatively light and I could even build a new one in a few days only!

It has also been very interesting to see the evolution of the ideas developed by the team on this experiment along the many weeks I visited the lab before the proper internship started.

Fun fact about diamonds and magnetism

In French, the word *diamant* and the word *aimant* (magnet) both come from the same ancient greek word $\alpha\delta\alpha\mu\alpha\varsigma$ (which meant indomitable)!

Appendix

Breakdown voltage of air and plasmas

One must be careful when using high voltage and low air pressure because one can reach the breakdown regime. The breakdown voltage follows the following law, called PASCHEN law:

$$V_b = \frac{Bpd}{C + \ln(pd)}$$

where

$$C = \ln\left(\frac{A}{\ln\left(1 + \frac{1}{\gamma}\right)}\right)$$

where A and B are experimentally measured constants, p is the pressure and d the distance between the electrodes and γ is the fluid heat capacity ratio ($\gamma = \frac{C_p}{C_v}$).

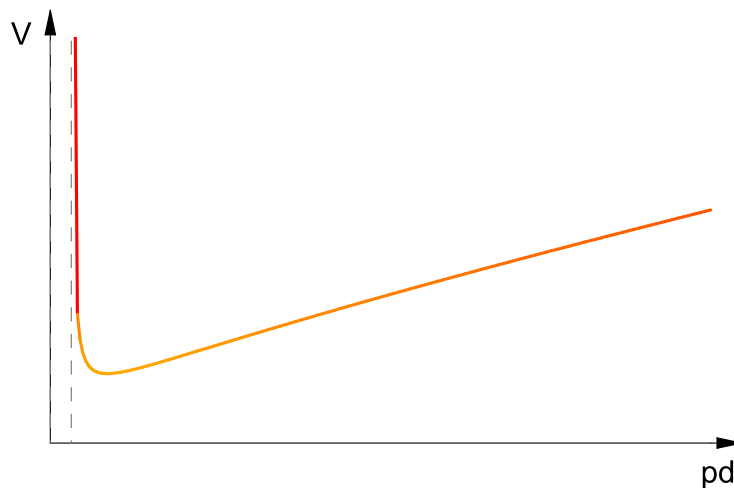


Figure 4.7: The evolution of the breakdown voltage as a function of the pd product.¹

In order to avoid creating a plasma inside the system, when we choose to work at low pressure, we must gradually, as the pressure drops, reduce the voltage amplitude applied to the PAUL trap. It has already happened that a plasma appears and it destroys the trap. The time to make an other decent trap is about half a day, but the process to make the new trap, to manage to trap a diamond with its new parameters and to go at low pressure is time consuming and should be avoided by being careful with low pressure experiments.

¹From <https://commons.wikimedia.org/wiki/File:Paschenkurve.svg>

Bibliography

- [1] C. Cohen-Tannoudji, B. Diu, F. Laloë, *Mécanique Quantique*, éd. Hermann, 1988
- [2] Tongcang Li, Simon Kheifets & Mark G. Raizen, *Millikelvin cooling of an optically trapped microsphere in vacuum*, Nature Physics volume **7**, pages 527–530 (2011)
- [3] G.M. Pančkov, *Druckabhängigkeit der Viskosität von Flüssigkeiten*, Žurnal fizičeskoj chimii. Moskova, **21** (1947), Nr 2, pages 187-195 (german translation)
- [4] Yoshihilo Arita, Michael Mazilu & Kishan Dholakia, *Laser-induced rotation and cooling of a trapped microgyroscope in vacuum*, Nature Communications volume **4**, Article number: 2374 (2013)
- [5] Veijola, T., Kuisma, H., Lahdenpera, J. & Ryhanen, T., *Equivalent-circuit model of the squeezed gas film in a silicon accelerometer*, Sensor Actuat. A Phys. **48**, 239–248 (1995)
- [6] A. Lenef & S. C. Rand, *Electronic structure of the N-V center in diamond: Theory*, Physical Review **B 53**, 13441-13455 (1996)
- [7] M. W. Doherty, N. B. Manson, P. Delaney & L. C. L. Hollenberg, *The negatively charged nitrogen-vacancy centre in diamond: the electronic solution*, New Journal of Physics, **13** 025019 (2011)
- [8] Anaïs Dréau. *Spins individuels dans le diamant pour l'information quantique*. Physique Quantique [quant-ph]. École normale supérieure de Cachan - ENS Cachan, 2013. Français. <NNT : 2013DENS0055>. <tel-01156590>
- [9] Maclaurin, D. and Doherty, M. W. and Hollenberg, L. C. L. and Martin, A. M., *Measurable Quantum Geometric Phase from a Rotating Single Spin*, Physical Review Letter, vol. **108** (2012), 108.240403
- [10] Sir Michael Victor Berry, *Quantal Phase Factors Accompanying Adiabatic Changes*, Proceedings of the Royal Society **A. 392** (1802): 45–57 (1984)
- [11] T. Delord, P. Huillery, L. Schwab, L. Nicolas, L. Lecordier, and G. Hétet, *Ramsey Interferences and Spin Echoes from Electron Spins Inside a Levitating Macroscopic Particle*, Phys. Rev. Lett. **121**, 053602 (2018)
- [12] T. Delord, L. Nicolas, Y. Chassagneux, and G. Hétet, *Strong coupling between a single nitrogen-vacancy spin and the rotational mode of diamonds levitating in an ion trap*, Phys. Rev. **A 96**, 063810 (2017) and other articles by the team.

Acknowledgements

I would like to thank Gabriel HÉTET for having me in his team working in the new yet simple and rich topic of NV-centres. I was happy to have the opportunity to join the team even before the internship started. I was amazed at seeing how Gabriel managed to make his experiment evolve thanks to his everlasting motivation.

I would like to thank Tom DELORD for his patience and friendliness when explaining me theoretical aspects of NV-centre physics.

I would like to thank Paul HUILLERY for his unexhaustable good mood and help getting familiar with the set-up and, of course, his LabView programs that were crucial for every measurement.

I would like to thank Louis NICOLAS for his kindness and for giving me unused optical items of his set-up in order to build mine and more particularly when he turned the compressor off!

I would like to thank all of the above for the time we spent talking not only about the experiment but also on general physics, motivations, work, PhD and much more.

I would also like to thank the rest of the *optique cohérente et non-linéaire* team downstairs that always welcomed me for the coffee break after lunch.